Research Article | Vol. 31, No. 10 / 8 May 2023 / Optics Express 16812
Optics EXPRESS

Enhancing underwater VLC with spatial division transmission and pairwise coding

JIWEI WANG,[1] CHEN CHEN,[1,*] BOHUA DENG,[2] ZHAOMING WANG,[3] MIN LIU,[1] AND H. Y. FU[2]

[1]School of Microelectronics and Communication Engineering, Chongqing University, Chongqing 400044, China
[2]Tsinghua Shenzhen International Graduate School, Tsinghua University, Shenzhen 518055, China
[3]Department of Engineering Science, University of Oxford, Oxford OX1 3PJ, UK
[*]c.chen@cqu.edu.cn

Abstract: In this paper, we propose and evaluate two spatial division transmission (SDT) schemes, including spatial division diversity (SDD) and spatial division multiplexing (SDM), for underwater visible light communication (UVLC) systems. Moreover, three pairwise coding (PWC) schemes, including two one-dimensional PWC (1D-PWC) schemes, i.e., subcarrier PWC (SC-PWC) and spatial channel PWC (SCH-PWC), and one two-dimensional PWC (2D-PWC) scheme are further applied for signal-to-noise ratio (SNR) imbalance mitigation in the UVLC systems using SDD and SDM with orthogonal frequency division multiplexing (OFDM) modulation. The feasibility and superiority of applying SDD and SDM with various PWC schemes in a practical bandlimited two-channel OFDM-based UVLC system have been verified through both numerical simulations and hardware experiments. The obtained results show that the performance of SDD and SDM schemes are largely determined by both the overall SNR imbalance and the system spectral efficiency. Moreover, the experimental results demonstrate the robustness of SDM with 2D-PWC against bubble turbulence. Specifically, SDM with 2D-PWC can obtain bit error rates (BERs) under the 7% forward error correction (FEC) coding limit of 3.8×10^{-3} with a probability higher than 96% for a signal bandwidth of 70 MHz and a spectral efficiency of 8 bits/s/Hz, achieving an overall data rate of 560 Mbits/s.

1. Introduction

The sixth generation (6G) networks are expected to offer ultra-high-capacity and ultra-low-latency communications covering space, air, ground and underwater environments [1]. With the ever-increasing demand for underwater activities such as ocean exploration, marine environmental monitoring and marine safety, underwater wireless communication (UWC) has been triggering tremendous attention from both academia and industry [2]. Recently, visible light communication (VLC), which has been recognized as one of the key enabling technologies for 6G, has been widely applied and investigated in underwater environments [3,4]. Compared with conventional UWC technologies such as underwater acoustic communication and underwater radio frequency communication, underwater VLC (UVLC) exhibits inherent advantages of large bandwidth, low propagation latency, high security, small size, low power consumption and low cost [5,6]. As a result, UVLC is generally considered as an effective complementary technology to conventional underwater acoustic communication for establishing efficient and robust communication links in underwater environments [7]. Lately, some LED-based UVLC systems have been demonstrated. For example, a 30-Mbps UVLC system using a chip-on-board LED array was demonstrated in [8], a LED-based UVLC system utilizing low-complexity sparse pruned-term-based nonlinear decision-feedback equalization was demonstrated in [9], and a blue-LED-based UVLC system using spatial diversity reception was demonstrated in [10].

#489530 https://doi.org/10.1364/OE.489530
Journal © 2023 Received 9 Mar 2023; revised 21 Apr 2023; accepted 24 Apr 2023; published 4 May 2023

Optics EXPRESS

Although UVLC has many advantages, applying UVLC in practical underwater environments still faces severe challenges such as imperfect transceiver alignment and turbulence [4,11]. Specifically, imperfect transceiver alignment is generally introduced by the random movements of transceivers in underwater environments due to ocean currents and wind, which inevitably reduces the optical power of the received optical signal [11,12]. Moreover, turbulence in UVLC channels is defined as the event that makes water experience rapid changes in the refractive index, which is commonly induced by the sudden variations in water temperature and pressure because of ocean currents or air bubbles [4,13]. It has been shown by the experimental measurements that turbulence can lead to significant amplitude fluctuation of the received signal and hence degrade the overall performance of UVLC systems [14,15]. By considering the high channel attenuation and random fading of received optical signals due to imperfect transceiver alignment and turbulence, it is of practical significance to propose efficient modulation, coding and transmission techniques to overcome these adverse underwater environmental factors.

1.1. Related work and motivation

So far, many techniques have been reported to enhance the performance of UVLC systems in the literature. Owing to its high spectral efficiency and resilience to inter-symbol interference and frequency-selective fading, orthogonal frequency-division multiplexing (OFDM) modulation has been generally adopted in UVLC systems [13,16]. Moreover, various coding schemes have also been introduced in UVLC systems. In [17] and [18], forward error correction (FEC) coding schemes such as Ross-Solomon (RS) code and convolutional code have been applied to improve the bit error rate (BER) performance of UVLC systems. In [19] and [20], pairwise coding (PWC) has been utilized to alleviate the signal-to-noise (SNR) imbalance in the frequency domain for UVLC systems. In addition, several pre-equalization schemes in the frequency and/or spatial domain have also been reported to mitigate the SNR imbalance [21,22]. However, compared with PWC, pre-equalization requires the additional knowledge of channel state information (CSI) at the transmitter side, which might also be vulnerable to LED nonlinearity as the low-SNR subcarriers might be allocated with an excessively high power [23].

Besides modulation and coding, different types of transmission schemes have also been considered in UVLC systems, such as single-input single-output (SISO), multiple-input single-output (MISO), single-input multiple-output (SIMO) and multiple-input multiple-output (MIMO).

1.1.1. SISO

SISO transmission can be seen as the simplest transmission scheme in UVLC systems, which only requires a single pair of transmitter and receiver. However, the transmission rate of SISO-UVLC systems is usually limited since only a single signal stream can be transmitted. To increase the transmission rate, polarization multiplexing and wavelength division multiplexing have been applied in SISO-UVLC systems [15,24–26]. Nevertheless, the transmission performance of SISO-UVLC systems can be significantly degraded by the adverse underwater environmental factors such as imperfect transceiver alignment and turbulence [4]. Hence, the reliability of SISO-UVLC systems might not be satisfactory in practical underwater environments.

1.1.2. MISO/SIMO

To enhance the reliability of SISO-UVLC systems, spatial diversity transmission has been adopted to replace the simple SISO transmission [27]. Specifically, spatial diversity can be exploited at the transmitter side through MISO transmission [28] or at the receiver side via SIMO transmission [29]. Although spatial diversity can efficiently offer diversity gain to enhance the transmission reliability, the transmission rate of MISO/SIMO-UVLC systems is still limited since the same signal is transmitted through all the spatial channels.

Optics EXPRESS

1.1.3. MIMO

By using multiple pairs of transceivers, MIMO transmission can be configured in UVLC systems [30–33]. To realize MIMO transmission, as illustrated in Fig. 1(a), the emission angle of each transmitter (e.g., LED) should be large enough such that its corresponding light spot at the receiver side can cover all the receivers. Nevertheless, a large emission angle inevitably leads to a much reduced light intensity at the receiver side, resulting in a significantly low receiving signal-to-noise ratio (SNR). Moreover, the mostly reported MIMO-UVLC systems have generally adopted a relatively simple MIMO scheme, i.e., spatial diversity, to harvest diversity gain and hence enhance the transmission reliability [31–33]. However, spatial multiplexing, which is much more spectral-efficient than spatial diversity, has been rarely applied in UVLC systems. The reason can be explained as follows: the transmission distance is generally much larger than the separation of adjacent transmitters or receivers in MIMO-UVLC systems, and hence the channel correction could be extremely high which greatly limits the achievable multiplexing gain.

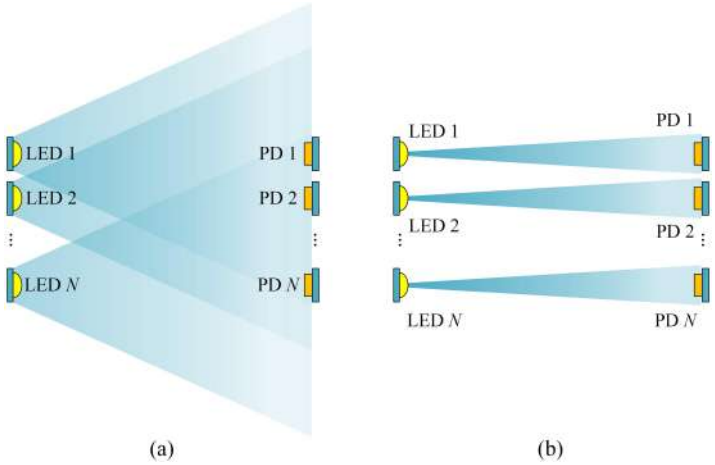

Fig. 1. Transceiver configuration of (a) conventional MIMO and (b) SDT.

To sum up, the existing transmission schemes cannot fully explore the spatial domain characteristic of UVLC systems to enable a high transmission rate. Moreover, how to achieve the trade-off between transmission reliability and rate in UVLC systems is still an open question, which is actually of practical significance for the deployment of UVLC systems in complex and dynamic underwater environments.

1.2. Main contributions

To substantially improve the transmission rate by exploiting the spatial domain characteristic of UVLC systems and further achieve a trade-off between transmission reliability and rate in practical underwater environments, we propose two spatial division transmission (SDT) schemes, i.e., spatial division diversity (SDD) and spatial division multiplexing (SDM), for UVLC systems. Differing from MIMO, as shown in Fig. 1(b), the proposed SDT schemes only need to establish multiple parallel point-to-point spatial channels, where the emission angle of each transmitter can be very small since the light spot of each transmitter only needs to cover the corresponding receiver within the same spatial channel. Hence, SDT allows the use of much more focused light beams and thus ensures much higher light intensity at the receiver side than MIMO, resulting in more superior SNR performance for SDT over MIMO. Moreover, by utilizing narrow-beam transmitters and spatially separated receivers, the proposed SDT schemes can be completely free

Optics EXPRESS

from channel correction, and therefore both diversity (i.e., SDD) and multiplexing (i.e., SDM) can be performed among multiple spatial channels. In addition, three PWC schemes are applied to further enhance the performance of UVLC systems employing the proposed SDT schemes. The main contributions of this work can be summarized as follows:

- Proposal of two SDT schemes for practical UVLC systems, including SDD and SDM, by establishing multiple parallel point-to-point spatial channels.
- Applying three PWC schemes, including two one-dimensional PWC (1D-PWC) schemes, i.e., subcarrier PWC (SC-PWC) and spatial channel PWC (SCH-PWC), and one two-dimensional PWC (2D-PWC) scheme, to efficiently mitigate SNR imbalance in OFDM-based UVLC systems using SDD and SDM.
- Presenting extensive simulation and experimental results to investigate and compare the performance of a practical bandlimited two-channel OFDM-based UVLC system using SDD and SDM with various PWC schemes.

1.3. Organization

The rest of this paper is organized as follows. The model of an OFDM-based UVLC system applying SDT and PWC is introduced in Section 2. Extensive simulation and experimental results are presented in Section 3. Finally, Section 4 gives the conclusion of the paper.

2. System model

In this section, we present the model of an OFDM-based UVLC system employing SDT and PWC, where the proposed two SDT schemes (i.e., SDD and SDM) are first introduced and then three PWC schemes (i.e., SC-PWC, SCH-PWC and 2D-PWC) are also discussed.

2.1. SDT

The principle of the proposed SDT schemes, including SDD and SDM, are first introduced as follows.

2.1.1. SDD

The block diagram of an OFDM-based UVLC system with N parallel spatial channels using SDD is shown in Fig. 2(a), where all the N spatial channels simultaneously transmit the same OFDM signal. At the transmitter side, the serial input data are first serial-to-parallel (S/P) converted and then the resultant parallel data are mapped into quadrature amplitude modulation (QAM) symbols. After that, PWC encoding is performed to mitigate the SNR imbalance of different data subcarriers due to the low-pass frequency response of the bandlimited UVLC system. In order to generate a real-valued OFDM signal, Hermitian symmetry (HS) is imposed before executing the inverse fast Fourier transform (IFFT), and parallel-to-serial (P/S) conversion is also conducted to generate a serial signal. Subsequently, the serial signal is split into N streams corresponding to N parallel spatial channels. Each digital signal stream is converted into an analog signal stream via digital-to-analog (D/A) conversion and a DC bias is further added to ensure the non-negativity of the analog signal stream. Finally, the obtained N analog, real-valued and non-negative signal streams are employed to modulate N LEDs for the N parallel spatial channels. After propagation through the water channel, N photo-detectors (PDs) are adopted to detect the N parallel optical signals at the receiver side. The detected analog signals are first converted into digital signals via analog-to-digital (A/D) conversion, and then maximum ratio combining (MRC) is applied for signal combination to generate a single output signal [34]. The resultant signal is further demodulated to obtain the final output data, and the demodulation procedures include S/P conversion, FFT, channel estimation, PWC decoding, QAM demapping

Optics EXPRESS

and P/S conversion. The detailed principle of PWC encoding and decoding with respect to different data subcarriers in the frequency domain will be introduced in the following subsection.

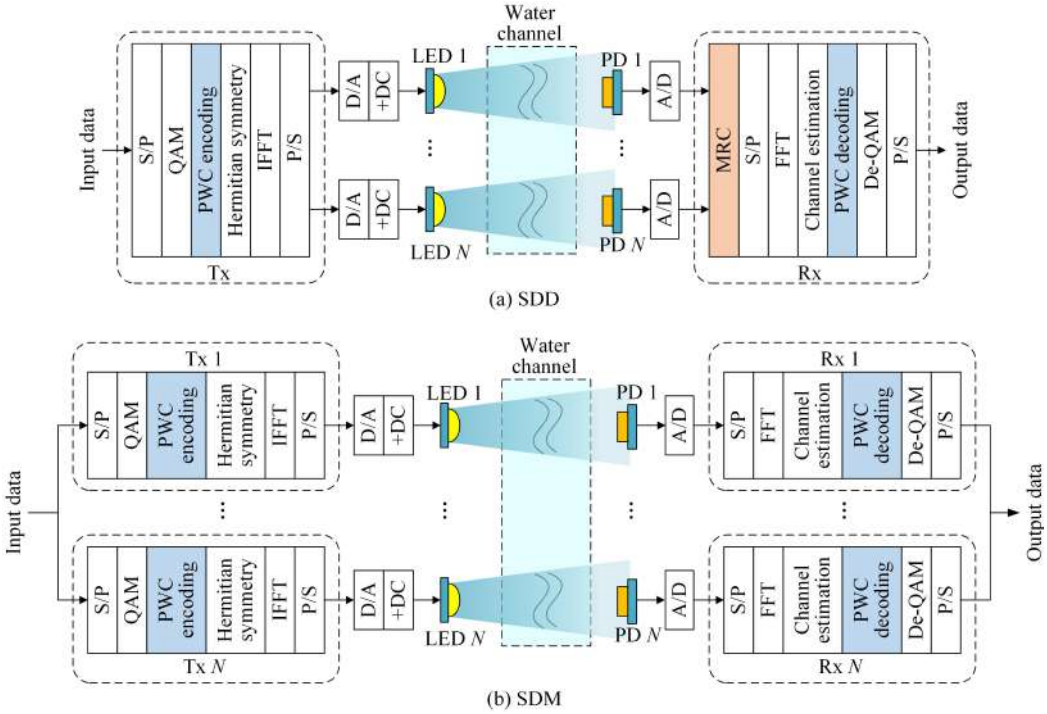

Fig. 2. Block diagram of OFDM-based UVLC using (a) SDD and (b) SDM.

Letting M_{SDD} represent the order of QAM constellation used in the OFDM-based N-channel SDD-UVLC system, the spectral efficiency over the effective signal bandwidth can be given by $\eta_{\mathrm{SDD}} = \log_2 M_{\mathrm{SDD}}$, which is exactly the same as that of the OFDM-based SISO-UVLC system applying the same constellation. It can be observed from Fig. 2(a) that the N-channel SDD-UVLC system only needs a single pair of OFDM transmitter and receiver modules, which is capable of harvesting diversity gain by applying SDD over the N parallel spatial channels.

2.1.2. SDM

The block diagram of an OFDM-based UVLC system with N parallel spatial channels using SDM is illustrated in Fig. 2(b), where all the N spatial channels transmit different OFDM signals. At the transmitter side, the input data are first split into N parallel data streams and each data stream is modulated into a serial OFDM signal. Hence, N digital real-valued parallel signal streams can be generated, which are further converted into N analog, real-valued and non-negative parallel signal streams for LED modulation via D/A conversion and DC bias addition. At the receiver side, the detected N parallel analog OFDM signals are first converted into digital signals via A/D conversion, which are then separately demodulated to recover the N output parallel data streams. The final output data can be obtained by combining the N output parallel data streams together.

Letting M_{SDM} denote the order of QAM constellation adopted in the OFDM-based N-channel SDM-UVLC system, the spectral efficiency over the effective signal bandwidth can be given by $\eta_{\mathrm{SDM}} = N \log_2 M_{\mathrm{SDM}}$. As we can see from Fig. 2(b), the N-channel SDM-UVLC system requires totally N pairs of OFDM transmitter and receiver modules, which can achieve multiplexing gain by applying SDM over the N parallel spatial channels. In the bandlimited N-channel UVLC

Optics EXPRESS

system, the received SNRs of different data subcarriers in each spatial channel might be different due to the low-pass frequency response of the system. Meanwhile, the overall received SNRs of different spatial channels might also be different, since different spatial channels might have different channel attenuation coefficients due to the adverse underwater environmental factors such as imperfect transceiver alignment and turbulence [4]. Therefore, SNR imbalance not only occurs in the frequency domain between different data subcarriers within each spatial channel, but also in the spatial domain between different spatial channels. In order to mitigate the SNR imbalance in both the frequency and spatial domains, efficient PWC schemes can be adopted, which will be described in detail in the following subsection.

2.2. PWC

As an efficient scheme to mitigate SNR imbalance, PWC can be applied among different data subcarriers in the frequency domain or among different spatial channels in the spatial domain [35–37], which can also be jointly utilized in both the frequency and spatial domains [38]. In the following, two 1D-PWC schemes, i.e., SC-PWC and SCH-PWC, are first introduced, and then a 2D-PWC scheme is further discussed.

2.2.1. 1D-PWC

To implement 1D-PWC, all the subcarriers or spatial channels should be paired first with the largest possible SNR imbalance, and then 1D-PWC, i.e., SC-PWC/SCH-PWC, is executed with respect to each subcarrier/spatial channel pair in the frequency/spatial domain.

For simplicity and without loss of generality, we assume all the spatial channels have the same number of data subcarriers and let N_{SC} denote the number of data subcarriers per spatial channel. On the one hand, due to the low-pass nature of practical UVLC systems, the subcarrier with a higher frequency usually has a smaller receiving SNR than that with a lower frequency. As a result, for SC-PWC, the N_{SC} data subcarriers are first divided into two groups: the first group contains the first half of the N_{SC} data subcarriers starting from subcarrier 1 to subcarrier $N_{SC}/2$, while the second group contains the second half starting from subcarrier $N_{SC}/2+1$ to subcarrier N_{SC}. Subsequently, a total of $N_{SC}/2$ subcarrier pairs can be obtained by pairing the m-th subcarrier in the first group and the $(N_{SC}-m+1)$-th subcarrier in the second group together, with $m = 1, 2, \ldots, N_{SC}/2$. On the other hand, practical UVLC systems generally have two types of channel conditions: one is static water channel with fixed channel attenuation coefficients, and the other is dynamic water channel with time-varying channel attenuation coefficients. For SCH-PWC over N static spatial channels, the spatial channels can be sorted according to the corresponding channel attenuation coefficients. For SCH-PWC over N dynamic spatial channels, it might not be feasible to sort the spatial channels by utilizing channel attenuation coefficients, since the channel attenuation coefficients might change with time very rapidly. Nevertheless, we can sort and pair the spatial channels according to their spatial locations to achieve the largest physical separation. Following the same manner as that for SC-PWC, the sorted N spatial channels can be divided into $N/2$ pairs and SCH-PWC can be performed with respect to each spatial channel pair.

The encoding and decoding procedures of 1D-PWC are depicted in Figs. 3(a) and (b), respectively. For 1D-PWC encoding, as shown in Fig. 3(a), angle rotation is first performed with respect to the input QAM symbols X_{m1} and X_{m2} of the m-th subcarrier pair or spatial channel pair, and the resultant rotated symbols X_{m1}^{rot} and X_{m2}^{rot} can be given by

$$\begin{cases} X_{m1}^{rot} = e^{j\theta} X_{m1} \\ X_{m2}^{rot} = e^{j\theta} X_{m2} \end{cases}, \tag{1}$$

Optics EXPRESS

where θ is the rotation angle, which is generally assumed to be 45° for a wide range of SNR imbalance [35,36]. After that, the in-phase (I) and quadrature (Q) components of X_{m1}^{rot} and X_{m2}^{rot} are interleaved, and the output symbols Y_{m1} and Y_{m2} can be obtained by

$$\begin{cases} Y_{m1} = \Re(X_{m1}^{rot}) + j\Re(X_{m2}^{rot}) \\ Y_{m2} = \Im(X_{m1}^{rot}) + j\Im(X_{m2}^{rot}) \end{cases}, \tag{2}$$

where $\Re(\cdot)$ and $\Im(\cdot)$ denote the operations to extract the I and Q components of a complex-valued input, respectively.

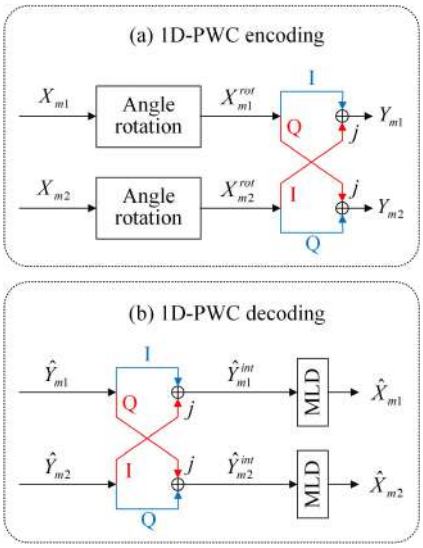

Fig. 3. Principle of 1D-PWC: (a) encoding and (b) decoding.

For 1D-PWC decoding, as can be seen from Fig. 3(b), I/Q de-interleaving is first executed with respect to the corresponding received symbols $\hat{Y}_{m1}$ and $\hat{Y}_{m2}$, and the resultant symbols $\hat{Y}_{m1}^{int}$ and $\hat{Y}_{m2}^{int}$ can be expressed by

$$\begin{cases} \hat{Y}_{m1}^{int} = \Re(Y_{m1}) + j\Re(Y_{m2}) \\ \hat{Y}_{m2}^{int} = \Im(Y_{m1}) + j\Im(Y_{m2}) \end{cases}. \tag{3}$$

Then, maximum likelihood detection (MLD) is applied with respect to $\hat{Y}_{m1}^{int}$ and $\hat{Y}_{m2}^{int}$ separately to recover the corresponding transmitted QAM symbols, which can be described by [35,38]

$$\begin{cases} \hat{X}_{m1} = \underset{C_{m1} \in \mathcal{A}}{\arg\min}\{\|\hat{Y}_{m1}^{int} - C_{m1}^{*}\|\} \\ \hat{X}_{m2} = \underset{C_{m2} \in \mathcal{A}}{\arg\min}\{\|\hat{Y}_{m2}^{int} - C_{m2}^{*}\|\} \end{cases}, \tag{4}$$

where $\|\cdot\|$ denotes the Euclidean norm operator, C_{m1} and C_{m2} are the constellation points in the adopted QAM constellation set $\mathcal{A}$, and C_{m1}^{*} and C_{m2}^{*} are given by

$$\begin{cases} C_{m1}^{*} = h_{m1}\Re\left(e^{j\theta}C_{m1}\right) + jh_{m2}\Im\left(e^{j\theta}C_{m1}\right) \\ C_{m2}^{*} = h_{m2}\Re\left(e^{j\theta}C_{m2}\right) + jh_{m1}\Im\left(e^{j\theta}C_{m2}\right) \end{cases}, \tag{5}$$

Optics EXPRESS

where h_{m1} and h_{m2} represent the channel attenuation coefficients of the two subcarriers/spatial channels in the m-th subcarrier/spatial channel pair.

2.2.2. 2D-PWC

In order to perform 2D-PWC, both the subcarriers and the spatial channels are first divided into pairs, and then a pair of subcarriers and a pair of spatial channels are jointly grouped to execute 2D-PWC in both the frequency and spatial domains. Figure 4 shows the principle of 2D-PWC, where $X_{c1,s1}$, $X_{c1,s2}$, $X_{c2,s1}$ and $X_{c2,s2}$ denote the four input QAM symbols of the s-th subcarrier pair and the c-th spatial channel pair, with $s = 1, 2, \ldots, N_{SC}/2$ and $c = 1, 2, \ldots, N/2$.

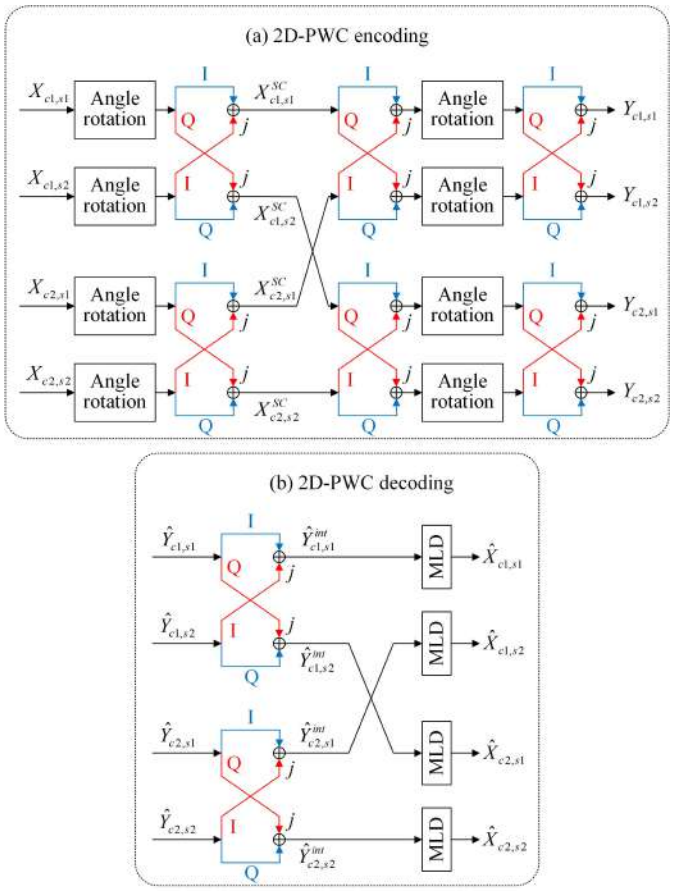

Fig. 4. Principle of 2D-PWC: (a) encoding and (b) decoding.

For 2D-PWC encoding, as shown in Fig. 4(a), angle rotation and interleaving are first sequentially conducted with respect to the input QAM symbols of the i-th spatial channel, i.e., $X_{i,s1}$ and $X_{i,s2}$ with $i \in \{c1, c2\}$, and the resultant symbols $X_{i,s1}^{\mathrm{SC}}$ and $X_{i,s2}^{\mathrm{SC}}$ can be given by

$$\begin{cases} X_{i,s1}^{\mathrm{SC}} = \Re(e^{j\varphi} X_{i,s1}) + j\Re(e^{j\varphi} X_{i,s2}) \\ X_{i,s2}^{\mathrm{SC}} = \Im(e^{j\varphi} X_{i,s1}) + j\Im(e^{j\varphi} X_{i,s2}) \end{cases}, \tag{6}$$

where φ denotes the rotation angle, which is also assumed to be 45° here. Then, interleaving, angle rotation and interleaving are further sequentially performed with respect to $X_{c1,k}$ and $X_{c2,k}$

Optics EXPRESS

of the k-th subcarrier with $k \in \{s1, s2\}$ to yield the 2D-PWC encoded symbols as follows [38]:

$$\begin{bmatrix} Y_{c1,k} \\ Y_{c2,k} \end{bmatrix} = \begin{bmatrix} \cos\varphi & -\sin\varphi \\ \sin\varphi & \cos\varphi \end{bmatrix} \times \begin{bmatrix} X^{\mathrm{SC}}_{c1,k} \\ X^{\mathrm{SC}}_{c2,k} \end{bmatrix}. \tag{7}$$

For 2D-PWC decoding, as can be seen from Fig. 4(b), de-interleaving is first carried out with respect to the received symbols $\hat{Y}_{i,s1}$ and $\hat{Y}_{i,s2}$ with $i \in \{c1, c2\}$, and the obtained symbols $\hat{Y}^{int}_{i,s1}$ and $\hat{Y}^{int}_{i,s2}$ are described by

$$\begin{cases} \hat{Y}^{int}_{i,s1} = \Re(\hat{Y}_{i,s1}) + j\Re(\hat{Y}_{i,s2}) \\ \hat{Y}^{int}_{i,s2} = \Im(\hat{Y}_{i,s1}) + j\Im(\hat{Y}_{i,s2}) \end{cases}. \tag{8}$$

Subsequently, MLD is separately employed with respect to $\hat{Y}^{int}_{i,s1}$ and $\hat{Y}^{int}_{i,s2}$ with $i \in \{c1, c2\}$ and the corresponding estimated QAM symbols can be obtained by

$$\begin{cases} \hat{X}_{i,s1} = \underset{C_{i,s1} \in \mathcal{A}'}{\arg\min}\{\|\hat{Y}^{int}_{i,s1} - C^{*}_{i,s1}\|\} \\ \hat{X}_{i,s2} = \underset{C_{i,s2} \in \mathcal{A}'}{\arg\min}\{\|\hat{Y}^{int}_{i,s2} - C^{*}_{i,s2}\|\} \end{cases}, \tag{9}$$

where $C_{i,s1}$ and $C_{i,s2}$ are the constellation points in the adopted QAM constellation set $\mathcal{A}'$, and $C^{*}_{i,s1}$ and $C^{*}_{i,s2}$ are given by

$$\begin{bmatrix} C^{*}_{i,s1} \\ C^{*}_{i,s2} \end{bmatrix} = H_i \times \begin{bmatrix} \cos\varphi & -\sin\varphi \\ \sin\varphi & \cos\varphi \end{bmatrix} \times \begin{bmatrix} e^{j\varphi}C_{i,s1} \\ e^{j\varphi}C_{i,s2} \end{bmatrix}, \tag{10}$$

where H_i represents the corresponding channel matrix, which is expressed by

$$H_i = \begin{bmatrix} h_{i,s1} & 0 \\ 0 & h_{i,s2} \end{bmatrix}. \tag{11}$$

3. Results and discussions

In this section, we evaluate and compare the performance of a practical OFDM-based UVLC system using different SDT and PWC schemes through numerical simulations and hardware experiments. In both simulations and experiments, we consider an OFDM-based UVLC system with two parallel spatial channels, where both spatial channels are bandlimited and exhibit low-pass characteristics. Moreover, the channel attenuation coefficients of two spatial channels are adjusted to reflect different static water channel conditions, and bubble turbulence is further generated in the experiments to emulate the dynamic water channel environment.

3.1. Simulation results

In the simulations, the additive noises of two spatial channels are both assumed to be additive white Gaussian noises (AWGNs). Moreover, the channel attenuation coefficient of the first spatial channel (i.e., CH_1) is fixed at $h_1 = 1$, while the channel attenuation coefficient of the second spatial channel (i.e., CH_2) is assumed to be $h_2 = 0.2$, 0.4 and 1. Hence, the channel ratio between CH_2 and CH_1 is given by $h_2/h_1 = 0.2$, 0.4 and 1. In addition, the measured electrical-optical-electrical (EOE) frequency response of two spatial channels in our established experimental UVLC system, as shown in Fig. 5, are adopted to model the low-pass characteristics of the two parallel spatial

Optics EXPRESS

channels. For performance evaluation and comparison, three transmission schemes including SISO, SDD and SDM are considered under two spectral efficiencies of 6 and 8 bits/s/Hz. The required QAM constellations for different schemes to achieve a target spectral efficiency are summarized in Table 1. To perform a fair comparison between SISO and SDD/SDM, the transmission power of the SISO-UVLC system is set to be twice as that of each individual spatial channel in the two-channel SDD/SDM-UVLC system.

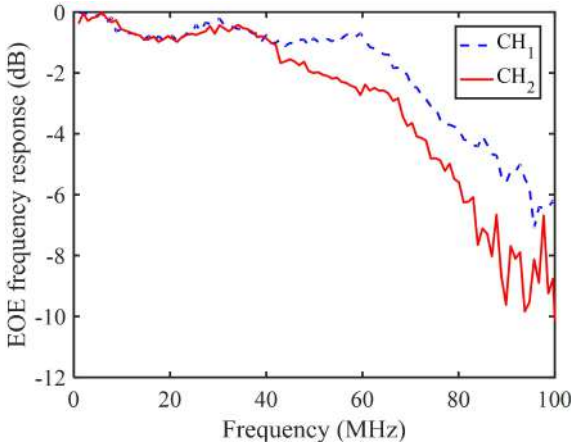

Fig. 5. Measured EOE frequency responses of two spacial channels in the experimental UVLC system.

Table 1. Required QAM Constellations for Different Transmission Schemes to Achieve a Target Spectral Efficiency.

Scheme	6 bits/s/Hz	8 bits/s/Hz
SISO	64-QAM	256-QAM
SDD	64-QAM	256-QAM
SDM	8-QAM	16-QAM

Figure 6 presents the simulated BER versus signal bandwidth for a spectral efficiency of 6 bits/s/Hz with different channel ratios. For the case of $h_2/h_1 = 0.2$, as shown in Fig. 6(a), the BER of SISO cannot reach the 7% FEC coding limit of 3.8×10^{-3} within the bandwidth range from 30 to 80 MHz. When SDM is employed, the maximum available bandwidth under the FEC coding limit is only 34.8 MHz. In contrast, the maximum available bandwidths are increased to 40.4, 56.5 and 67.9 MHz for SDM with SC-PWC, SCH-PWC and 2D-PWC, respectively. When compared with SDM without PWC, a slight bandwidth extension of 5.6 MHz is obtained when SC-PWC is applied in SDM. However, a substantial bandwidth extension of 21.7 MHz is achieved by applying SCH-PWC in SDM. In comparison to SDM with SCH-PWC, a further 11.4-MHz bandwidth extension can be attained by SDM with 2D-PWC. Moreover, SDD obtains a comparable maximum available bandwidth as SDM with 2D-PWC, while SDD with SC-PWC achieves a maximum available bandwidth of 75.6 MHz, which is the largest among all the considered schemes. For the case of $h_2/h_1 = 0.4$, as shown in Fig. 6(b), SISO still performs the worst, while SDD and SDM can obtain comparable BER performance. Furthermore, SDM with SC-PWC slightly outperforms SDM with SCH-PWC, and SDM with 2D-PWC achieves the best performance. For the case of $h_2/h_1 = 1$, as can be seen from Fig. 6(c), the two spatial channels have the same channel attenuation coefficients and hence SISO and SDD have exactly

Optics EXPRESS

the same performance. Since there is no channel difference, the use of SCH-PWC cannot bring any performance improvement. Hence, SDM with SCH-PWC performs the same as SDM, and SDM with 2D-PWC also performs the same as SDM with SC-PWC. It can be clearly observed from Figs. 6(a), (b) and (c) that the SDD schemes outperform the SDM schemes when the channel ratio is relatively small, i.e., the SNR imbalance due to channel difference in the spatial domain is much more significant than that caused by subcarrier difference in the frequency domain, and the SDM schemes perform better than the SDD schemes when the channel ratio is relatively large, i.e., the SNR imbalance due to subcarrier difference in the frequency domain becomes dominant. The simulated BER versus signal bandwidth for a spectral efficiency of 8 bits/s/Hz with different channel ratios is shown in Fig. 7. For a relatively small gain ratio of $h_2/h_1 = 0.2$, as can be seen from Fig. 7(a), the SDD schemes perform better than SDM and SDM with SC-PWC, but worse than SDM with SCH-PWC or 2D-PWC. When the channel ratio becomes larger, as shown in Figs. 7(b) and (c), the SDM schemes generally outperform the SDD schemes. By comparing Figs. 6 and 7, we can conclude that the performance of the SDM schemes becomes much more superior when the two-channel UVLC system has a higher spectral efficiency.

Figure 8 shows the simulated BER versus channel ratio h_2/h_1 for different signal bandwidths and spectral efficiencies. As we can see, with the increase of channel ratio, the performance gap between SISO and SDD becomes gradually reduced and the performance improvement of applying SC-PWC in SDD becomes much more significant. It can also be found that the BERs of SDD schemes are only slightly increased when the channel ratio is reduced from 1 to 0.1, suggesting the inherent tolerance of SDD schemes against the SNR imbalance induced by channel difference. Furthermore, the tolerable channel ratio of SDM can be substantially reduced by adopting the PWC schemes. Specifically, for a signal bandwidth of 80 MHz and a spectral efficiency of 6 bits/s/Hz, as shown in Fig. 8(a), the tolerable channel ratio is reduced from 0.54 to 0.27 by applying 2D-PWC in SDM, demonstrating the capability of 2D-PWC to efficiently mitigate the SNR imbalance caused by channel difference in the SDM-UVLC system.

3.2. Experimental results

We further conduct hardware experiments to investigate and compare the performance of a practical OFDM-based two-channel UVLC system applying SDD and SDM with different PWC schemes. In order to reflect a more practical underwater environment, two types of water channels are considered in the experiments: 1) static water channel with a fixed channel ratio, and 2) dynamic water channel with bubble turbulence. Figure 9 depicts the experimental setup of the hardware testbed, where the two parallel spatial channels are established by utilizing two pairs of commercially available VLC transmitter/receiver modules (HCCLS2021MOD01-Tx/Rx). The adopted Tx/Rx modules are highly integrated modules, which are suitable for the fast establishment of point-to-point VLC links. For more details about the Tx/Rx modules, please refer to our previous work [39]. Moreover, a 1-m water tank filled with tap water is adopted to emulate the water channel. The insets (a), (b) and (c) in Fig. 9 show the photos of the transmitter side, the overall system and the receiver side, respectively. At the transmitter side, the two transmitted signals are first generated offline by MATLAB, which are then loaded into a two-channel arbitrary waveform generator (AWG, Tektronix AFG31102), each channel with a sampling rate of 250 MSa/s and a peak-to-peak voltage of 250 mV. Subsequently, the two outputs of AWG are sent to the AC ports of two transmitter modules, and each transmitter module is driven by a 12-V DC voltage. At the receiver side, two receiver modules are used to receive the optical signals emitted by two transmitter modules, and each receiver module is also driven by a 12-V DC voltage. Subsequently, the output signals of two receiver modules are recorded by a two-channel digital storage oscilloscope (DSO, Tektronix MDO32) with a sampling rate of 1.25 GSa/s, which are further processed offline by MATLAB. During experimental measurements, three channel ratios of 0.2, 0.4 and 1 are considered for the static water channel by adjusting the

Optics EXPRESS

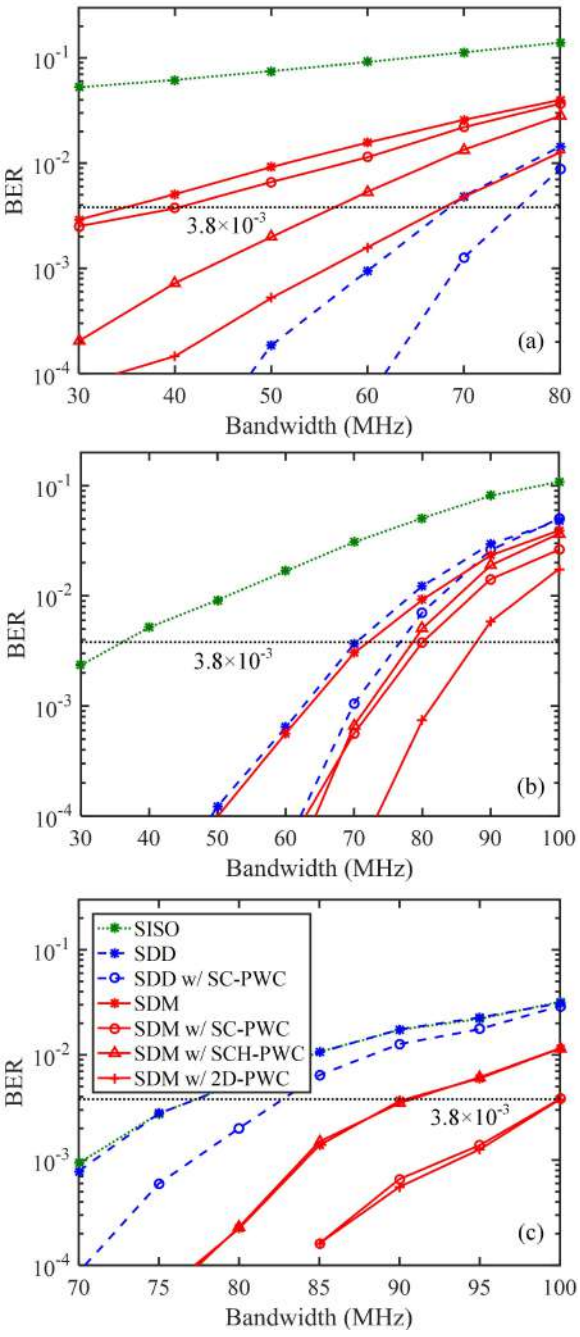

Fig. 6. Simulated BER vs. signal bandwidth for a spectral efficiency of 6 bits/s/Hz with different channel ratios: (a) $h_2/h_1 = 0.2$, (b) $h_2/h_1 = 0.4$, and (c) $h_2/h_1 = 1$.

Optics EXPRESS

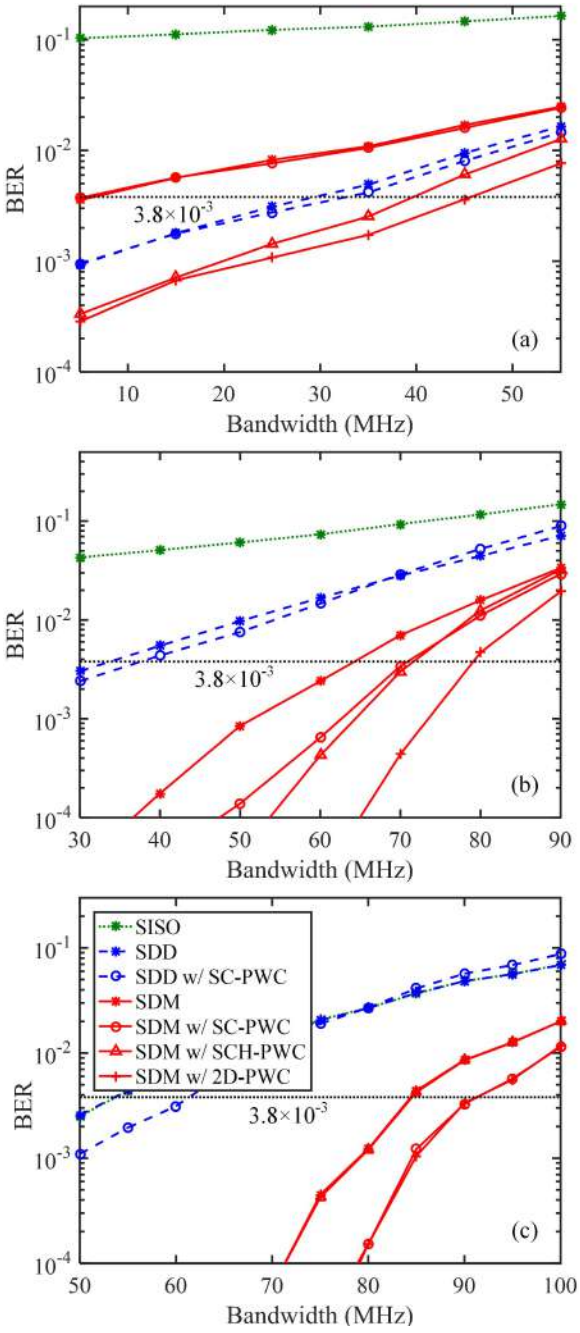

Fig. 7. Simulated BER vs. signal bandwidth for a spectral efficiency of 8 bits/s/Hz with different channel ratios: (a) $h_2/h_1 = 0.2$, (b) $h_2/h_1 = 0.4$, and (c) $h_2/h_1 = 1$.

Optics EXPRESS

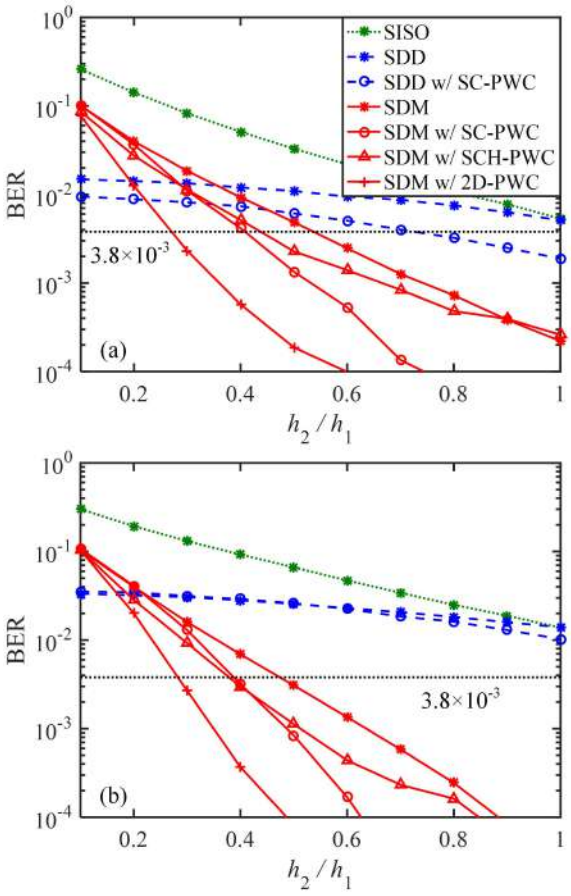

Fig. 8. Simulated BER vs. channel ratio h_2/h_1 for different signal bandwidths and spectral efficiencies: (a) 80 MHz, 6 bits/s/Hz and (b) 70 MHz, 8 bits/s/Hz.

signal reception of two receiver modules, while an air pump and a bubble strip are used together to generate the bubble turbulence for the dynamic water channel.

3.2.1. Static water channel with a fixed channel ratio

Figures 10 and 11 depict the experimental BER versus signal bandwidth with different channel ratios for spectral efficiencies of 6 and 8 bits/s/Hz, respectively. For the spectral efficiency of 6 bits/s/Hz with a channel ratio of 0.2, as shown in Fig. 10(a), the SDD schemes outperform the SDM schemes. Particularly, the largest maximum available bandwidth of 48.8 MHz is achieved by SDD with SC-PWC, which is corresponding to an overall data rate of 292.8 Mbits/s achieved by the OFDM-based two-channel UVLC system with a fixed channel ratio of 0.2. For the spectral efficiency of 6 bits/s/Hz with channel ratios of 0.4 and 1, the maximum available bandwidths are both obtained by SDM with 2D-PWC, which are 79.3 and 87.9 MHz, respectively. Hence, the overall achievable data rates of the OFDM-based two-channel UVLC system with fixed channel ratios of 0.4 and 1 are 475.8 and 527.4 Mbits/s, respectively. Moreover, for the spectral efficiency of 8 bits/s/Hz, as shown in Figs. 11(a)-(c), the largest maximum available bandwidth is always achieved by SDM with 2D-PWC for three channel ratios. It can be found that, for the channel ratios of 0.2, 0.4 and 1, the largest maximum available bandwidths obtained by SDM with 2D-PWC are 25.4, 74.2 and 86.1 MHz, respectively. Therefore, the overall achievable

Optics EXPRESS

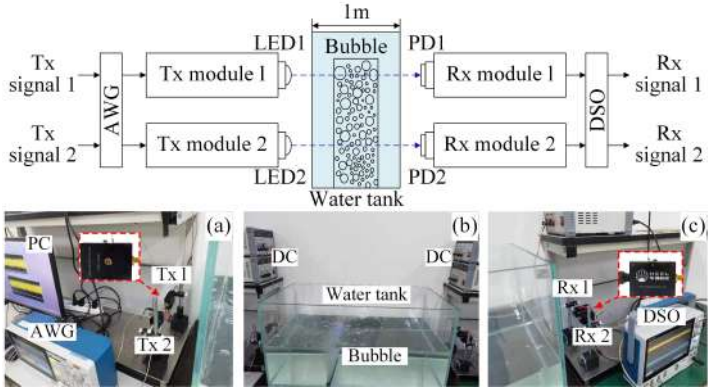

Fig. 9. Experimental setup of the two-channel UVLC system using two pairs of commercially available Tx and Rx modules. Insets: photos of (a) the Tx side, (b) the overall system, and (c) the Rx side.

data rates of the OFDM-based two-channel UVLC system with fixed channel ratios of 0.2, 0.4 and 1 are 203.2, 593.6 and 688.8 Mbits/s, respectively. Clearly, the same conclusion can be obtained from the experimental results as that from the simulation results for the OFDM-based two-channel UVLC system using SDD and SDM with different PWC schemes through the static water channel with a fixed channel ratio.

3.2.2. Dynamic water channel with bubble turbulence

Figure 12 depicts the estimated SNRs of two spatial channels at different measurements under bubble turbulence with a signal bandwidth of 70 MHz and a spectral efficiency of 8 bits/s/Hz, which is corresponding to an overall data rate of 560 Mbits/s. It can be seen that the SNR of each spatial channel suffers from notable fluctuations, and the SNRs of two parallel spatial channels are generally different at most of the measurements. Moreover, the probability that both two spatial channels simultaneously have low SNRs is found to be very small, and this observation directly confirms the advantage of parallel spatial division transmission over SISO transmission. Although clear SNR gaps can be observed for two parallel spatial channels at most of the measurements, the maximum SNR gap is only around 3 dB, which is mainly limited by the bubble generator employed in our experiments.

Figure 13 shows the average BER versus signal bandwidth for different schemes under bubble turbulence with a spectral efficiency of 8 bits/s/Hz. As we can see, the SDD schemes do not perform well and the reason is that the SNR imbalance caused by bubble turbulence is not very significant. In contrast, the SDM schemes can generally achieve satisfactory performance. Similarly, due to the insignificant SNR imbalance induced by bubble turbulence, SDM with SCH-PWC obtains nearly the same average BER performance as SDM without PWC. However, it is very interesting to find out that, although SDM and SCH-PWC perform comparably, SDM with 2D-PWC can outperform SDM with SC-PWC in a certain degree. This observation can be explained as follows: although the bubble turbulence-induced SNR imbalance is not significant itself, it can enlarge the overall SNR imbalance and hence bring performance gain to 2D-PWC over SC-PWC, as the overall SNR imbalance is jointly determined by both the low-pass-induced SNR imbalance within each spatial channel and the bubble turbulence-induced SNR imbalance among two spatial channels.

Figure 14 shows the cumulative distribution function (CDF) plot of measured BERs for different SDM schemes under bubble turbulence with different signal bandwidths. For a signal bandwidth of 60 MHz, as shown in Fig. 14(a), the probability for SDM without PWC to obtain

Optics EXPRESS

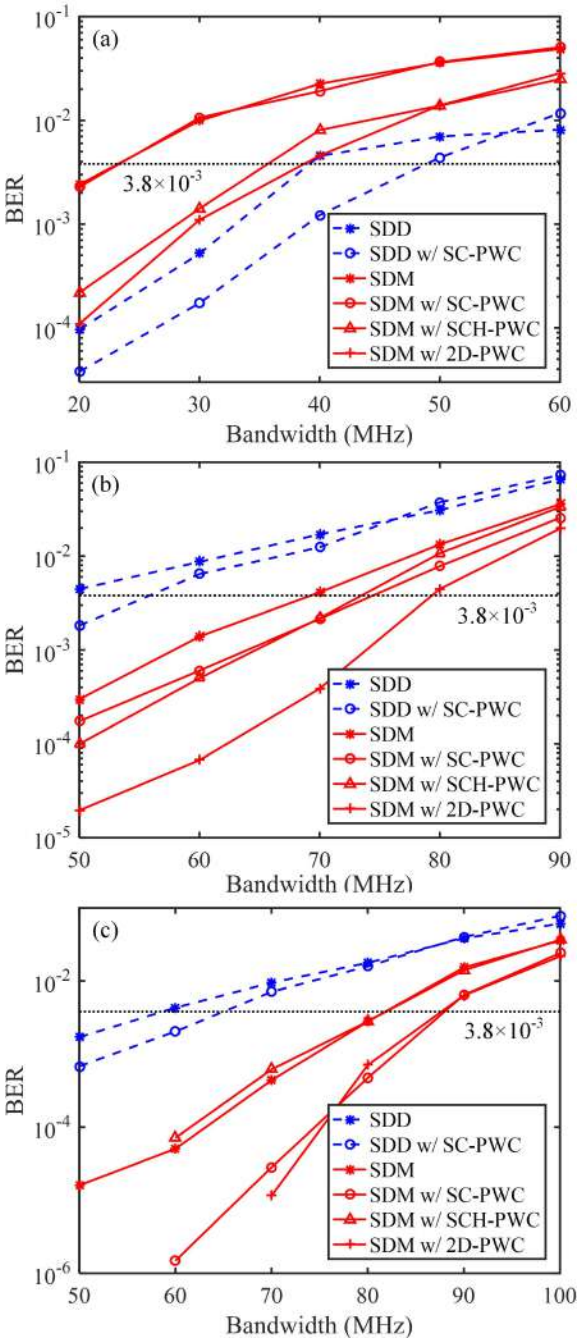

Fig. 10. Experimental BER vs. signal bandwidth for a spectral efficiency of 6 bits/s/Hz with different channel ratios: (a) $h_2/h_1 = 0.2$, (b) $h_2/h_1 = 0.4$, and (c) $h_2/h_1 = 1$.

Optics EXPRESS

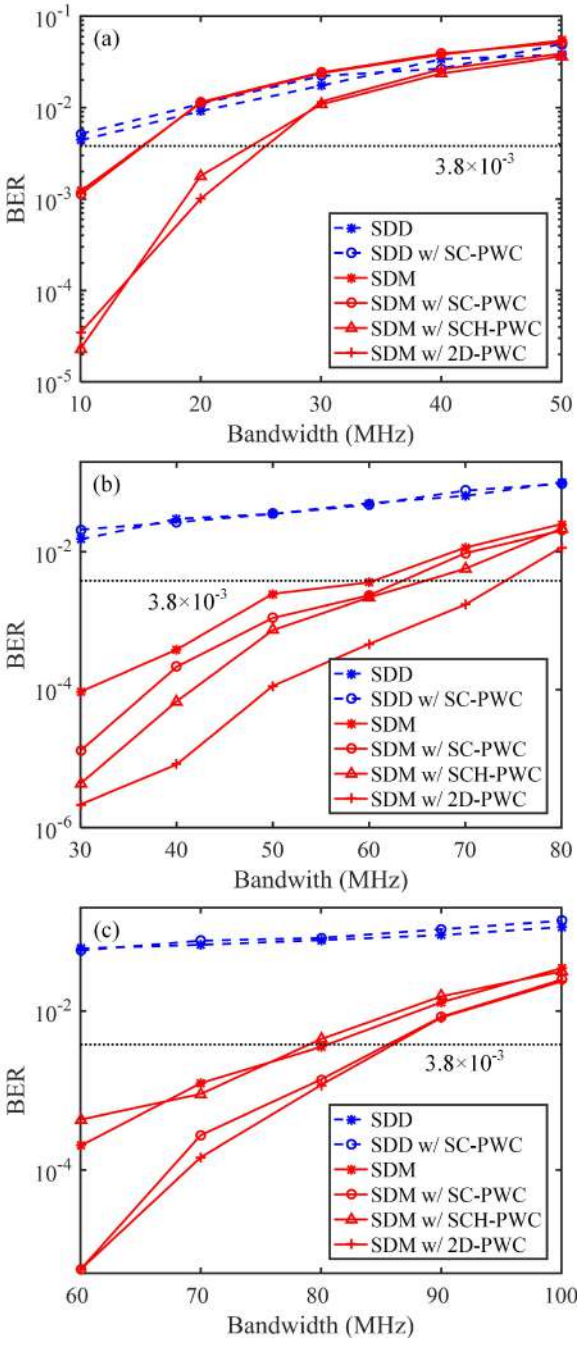

Fig. 11. Experimental BER vs. signal bandwidth for a spectral efficiency of 8 bits/s/Hz with different channel ratios: (a) $h_2/h_1 = 0.2$, (b) $h_2/h_1 = 0.4$, and (c) $h_2/h_1 = 1$.

Optics EXPRESS

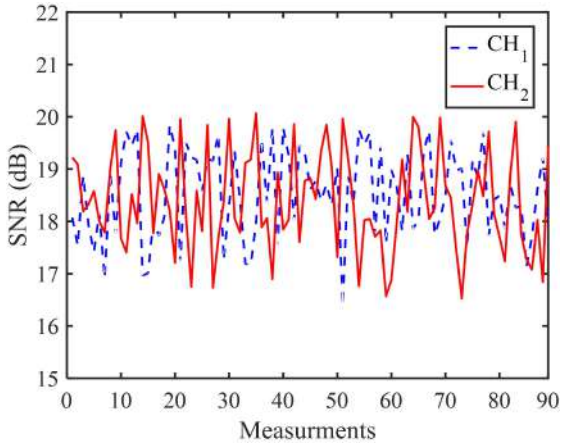

Fig. 12. Estimated SNRs of two spatial channels at different measurements under bubble turbulence.

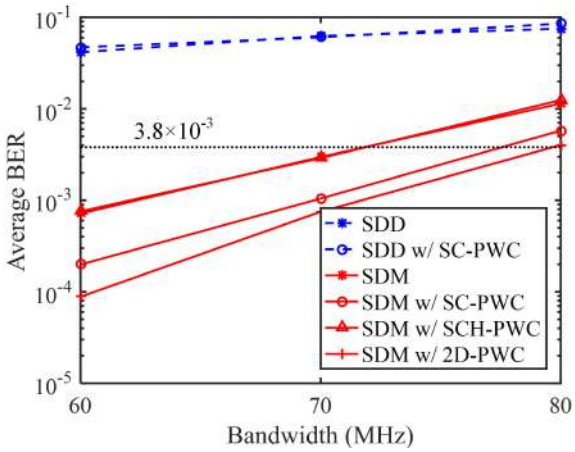

Fig. 13. Average BER vs. signal bandwidth for different schemes under bubble turbulence.

BERs under the 7% FEC coding limit of 3.8×10^{-3} is 98.9%, while all the three PWC-enhanced SDM schemes can achieve BERs under 3.8×10^{-3} with a probability 100%. When the signal bandwidth is increased to 70 MHz, the probabilities for SDM and SDM with SCH-PWC to obtain BERs under 3.8×10^{-3} are both about 80%, while SDM with SC-PWC or 2D-PWC can achieve BERs under 3.8×10^{-3} with a probability higher than 96%. For a relatively large signal bandwidth of 80 MHz, both SDM and SDM with SCH-PWC cannot obtain BERs under 3.8×10^{-3}, i.e., the probabilities are both zero. In contrast, SDM schemes with SC-PWC and 2D-PWC can still achieve BERs under 3.8×10^{-3}, and the corresponding probabilities are 26.9% and 56.2%, respectively. The outage probabilities of different SDM schemes under bubble turbulence for different signal bandwidths are provided in Table 2. Therefore, SDM with 2D-PWC is shown to be the most reliable scheme against bubble turbulence in the dynamic water channels for practical UVLC systems.

Optics EXPRESS

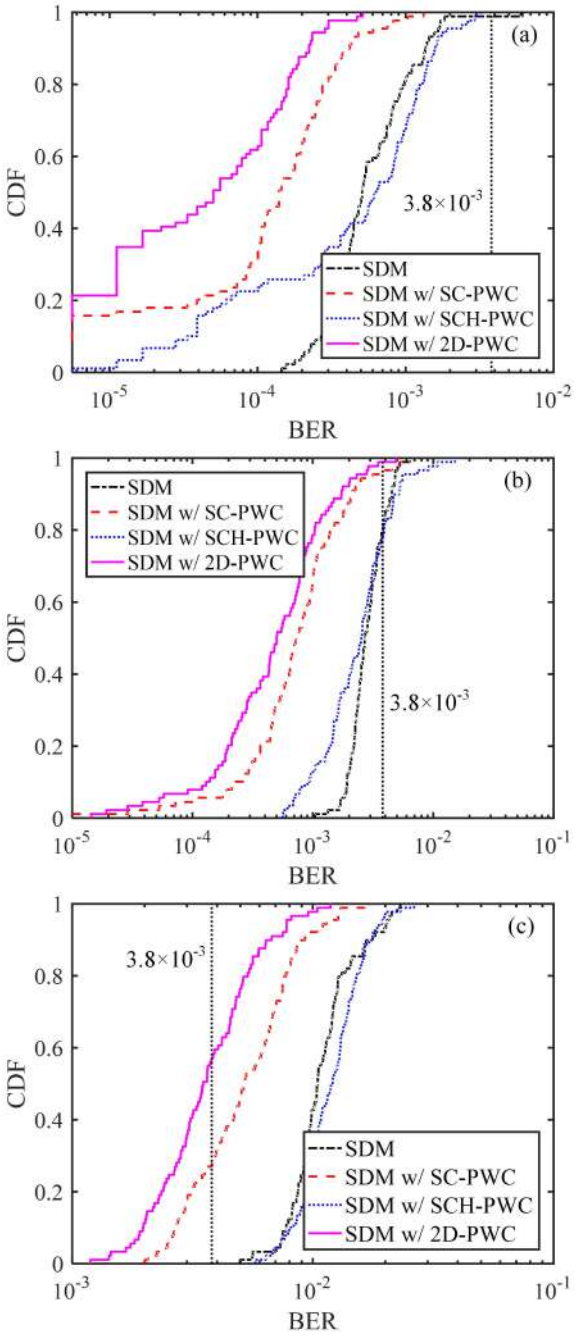

Fig. 14. CDF plot of measured BERs for different SDM schemes under bubble turbulence with different signal bandwidths: (a) 60 MHz, (b) 70 MHz, and (c) 80 MHz.

Optics EXPRESS

Table 2. Measured Outage Probabilities of Different SDM Schemes Under Bubble Turbulence.

Scheme	60 MHz	70 MHz	80 MHz
SDM	1.1%	20.2%	100%
SDM w/ SC-PWC	0%	3.4%	73.0%
SDM w/ SCH-PWC	0%	22.4%	100%
SDM w/ 2D-PWC	0%	1.1%	43.8%

4. Conclusion

In this paper, we have proposed and investigated two SDT schemes (i.e., SDD and SDM) for UVLC systems. Moreover, three PWC schemes, including two 1D-PWC schemes (i.e., SC-PWC and SCH-PWC) and a 2D-PWC scheme, have been further adopted to mitigate SNR imbalance in OFDM-based UVLC systems applying SDD and SDM. Both simulations and experiments have been conducted to evaluate and compare the performance of a practical bandlimited two-channel OFDM-based UVLC system using different SDT and PWC schemes under various channel conditions. For the static water channel with a fixed channel ratio, the simulation and experimental results reveal that the SDD schemes outperform the SDM schemes when the SNR imbalance is dominated by channel difference in the spatial domain and the spectral efficiency is relatively low, while the SDM schemes perform better than the SDD schemes when the SNR imbalance is dominated by subcarrier difference in the frequency domain and the spectral efficiency is relatively high. Furthermore, for the dynamic water channel with bubble turbulence, the experimental results demonstrate that SDM with 2D-PWC exhibits excellent robustness against bubble turbulence. In conclusion, the combination of SDT and PWC can be a promising candidate for UVLC systems to achieve a high transmission rate and further realize the trade-off between transmission reliability and rate in practical underwater applications.

Funding. National Natural Science Foundation of China (61901065, 62271091); Natural Science Foundation of Chongqing (cstc2021jcyj-msxmX0480).

Disclosures. The authors declare no conflicts of interest.

Data availability. The data underlying the results presented in this paper are not publicly available at this time but may be obtained from the authors upon reasonable request.

References

1. Z. Zhang, Y. Xiao, Z. Ma, M. Xiao, Z. Ding, X. Lei, G. K. Karagiannidis, and P. Fan, "6G wireless networks: Vision, requirements, architecture, and key technologies," IEEE Veh. Technol. Mag. **14**(3), 28–41 (2019).
2. C. M. Gussen, P. S. Diniz, M. L. Campos, W. A. Martins, F. M. Costa, and J. N. Gois, "A survey of underwater wireless communication technologies," J. Commun. Inf. Sys. **31**(1), 242–255 (2016).
3. N. Chi, Y. Zhou, Y. Wei, and F. Hu, "Visible light communication in 6G: Advances, challenges, and prospects," IEEE Veh. Technol. Mag. **15**(4), 93–102 (2020).
4. Z. Zeng, S. Fu, H. Zhang, Y. Dong, and J. Cheng, "A survey of underwater optical wireless communications," IEEE Commun. Surveys Tuts. **19**(1), 204–238 (2017).
5. G. Cossu, R. Corsini, A. Khalid, S. Balestrino, A. Coppelli, A. Caiti, and E. Ciaramella, "Experimental demonstration of high speed underwater visible light communications," in *Proc. IEEE Int. Workshops Opt. Wireless Commun. (IWOW)*, (2013), pp. 11–15.
6. M. Elamassie, F. Miramirkhani, and M. Uysal, "Performance characterization of underwater visible light communication," IEEE Trans. Commun. **67**(1), 543–552 (2019).
7. M. F. Ali, D. N. K. Jayakody, and Y. Li, "Recent trends in underwater visible light communication (UVLC) systems," IEEE Access **10**, 22169–22225 (2022).
8. B. Han, J. Yang, K. Sun, Y. Sun, and B. Zhang, "Experimental demonstration of blue light transmitter with 30 Mbps modulated rate and 1.69 W optical power for underwater wireless optical communication based on chip-on-board light-emitting diode array," Opt. Eng. **61**(05), 056106 (2022).
9. C. Fei, R. Chen, J. Du, Y. Wang, J. Tian, G. Zhang, J. Zhang, X. Hong, and S. He, "Underwater wireless optical communication utilizing low-complexity sparse pruned-term-based nonlinear decision-feedback equalization," Appl. Opt. **61**(22), 6534–6543 (2022).

Optics EXPRESS

10. R. Chen, J. Du, Y. Wang, C. Fei, T. Zhang, J. Tian, G. Zhang, X. Hong, and S. He, "Experimental demonstration of real-time optical DFT-S DMT signal transmission for a blue-LED-based UWOC system using spatial diversity reception," Appl. Opt. **62**(3), 541–551 (2023).
11. S. Arnon, "Underwater optical wireless communication network," Opt. Eng. **49**(1), 015001 (2010).
12. I. C. Ijeh, M. A. Khalighi, and S. Hranilovic, "Parameter optimization for an underwater optical wireless vertical link subject to link misalignments," IEEE J. Ocean. Eng. **46**(4), 1424–1437 (2021).
13. H. Jiang, H. Qiu, N. He, W. Popoola, Z. Ahmad, and S. Rajbhandari, "Performance of spatial diversity DCO-OFDM in a weak turbulence underwater visible light communication channel," J. Lightwave Technol. **38**(8), 2271–2277 (2020).
14. Z. Vali, A. Gholami, Z. Ghassemlooy, M. Omoomi, and D. G. Michelson, "Experimental study of the turbulence effect on underwater optical wireless communications," Appl. Opt. **57**(28), 8314–8319 (2018).
15. L. Zhang, Z. Wang, Z. Wei, C. Chen, G. Wei, H. Fu, and Y. Dong, "Towards a 20 Gbps multi-user bubble turbulent NOMA UOWC system with green and blue polarization multiplexing," Opt. Express **28**(21), 31796–31807 (2020).
16. S. Hessien, S. C. Tokgöz, N. Anous, A. Boyacı, M. Abdallah, and K. A. Qaraqe, "Experimental evaluation of OFDM-based underwater visible light communication system," IEEE Photonics J. **10**(5), 1–13 (2018).
17. P. Wang, C. Li, and Z. Xu, "A cost-efficient real-time 25 Mb/s system for LED-UOWC: design, channel coding, FPGA implementation, and characterization," J. Lightwave Technol. **36**(13), 2627–2637 (2018).
18. S. K. Mahapatra and S. K. Varshney, "Performance of the Reed-Solomon-coded underwater optical wireless communication system with orientation-based solar light noise," J. Opt. Soc. Am. A **39**(7), 1236–1245 (2022).
19. C. T. Geldard, E. Guler, A. Hamilton, and W. O. Popoola, "An empirical comparison of modulation schemes in turbulent underwater optical wireless communications," J. Lightwave Technol. **40**(7), 2000–2007 (2022).
20. J. He, L. Xu, and Y. Xiao, "Performance comparison of different rotated QAM based DMT schemes in underwater optical wireless communication," J. Lightwave Technol. (2022).
21. Y.-F. Liu, Y. C. Chang, C.-W. Chow, and C.-H. Yeh, "Equalization and pre-distorted schemes for increasing data rate in in-door visible light communication system," in *Proc. Opt. Fiber Commun. Conf. (OFC)*, (2011).
22. C. Chen and W.-D. Zhong, "Hybrid space-frequency domain pre-equalization for DC-biased optical orthogonal frequency division multiplexing based imaging multiple-input multiple-output visible light communication systems," Opt. Eng. **56**(3), 036102 (2017).
23. C. Chen, Y. Nie, M. Liu, Y. Du, R. Liu, Z. Wei, H. Fu, and B. Zhu, "Digital pre-equalization for OFDM-based VLC systems: Centralized or distributed?" IEEE Photonics Technol. Lett. **33**(19), 1081–1084 (2021).
24. L. Gai, X. Hei, Q. Zhu, Y. Yu, Y. Yang, F. Chen, Y. Gu, G. Wang, and W. Li, "Underwater wireless optical communication employing polarization multiplexing modulation and photon counting detection," Opt. Express **30**(24), 43301–43316 (2022).
25. M. Kong, W. Lv, T. Ali, R. Sarwar, C. Yu, Y. Qiu, F. Qu, Z. Xu, J. Han, and J. Xu, "10-m 9.51-Gb/s RGB laser diodes-based WDM underwater wireless optical communication," Opt. Express **25**(17), 20829–20834 (2017).
26. F. Hu, G. Li, P. Zou, J. Hu, S. Chen, Q. Liu, J. Zhang, F. Jiang, S. Wang, and N. Chi, "20.09-Gbit/s underwater WDM-VLC transmission based on a single Si/GaAs-substrate multichromatic LED array chip," in *Proc. Opt. Fiber Commun. Conf. (OFC)*, (2020).
27. Y. Wei, B. Lin, X. Tang, Y. Li, M. Zhang, Z. Ghassemlooy, Y. Wu, and H. Li, "Underwater visible light communications based on spatial diversity," in *Proc. Int. Conf. Opt. Commun. Netw. (ICOCN)*, (2017), pp. 1–3.
28. M. A. A. Ali, "Investigation of multiple input–single output technique for wireless optical communication system under coastal water," Opt. Quant. Electron. **52**(9), 416 (2020).
29. W. Liu, Z. Xu, and L. Yang, "SIMO detection schemes for underwater optical wireless communication under turbulence," Photonics Res. **3**(3), 48–53 (2015).
30. Y. Song, W. Lu, B. Sun, Y. Hong, F. Qu, J. Han, W. Zhang, and J. Xu, "Experimental demonstration of MIMO-OFDM underwater wireless optical communication," Opt. Commun. **403**, 205–210 (2017).
31. M. V. Jamali, J. A. Salehi, and F. Akhoundi, "Performance studies of underwater wireless optical communication systems with spatial diversity: MIMO scheme," IEEE Trans. Commun. **65**(3), 1176–1192 (2017).
32. M. V. Jamali, P. Nabavi, and J. A. Salehi, "MIMO underwater visible light communications: Comprehensive channel study, performance analysis, and multiple-symbol detection," IEEE Trans. Veh. Technol. **67**(9), 8223–8237 (2018).
33. J. Li, D. Ye, K. Fu, L. Wang, J. Piao, and Y. Wang, "Single-photon detection for MIMO underwater wireless optical communication enabled by arrayed LEDs and SiPMs," Opt. Express **29**(16), 25922–25944 (2021).
34. C. Chen, W.-D. Zhong, H. Yang, S. Zhang, and P. Du, "Reduction of SINR fluctuation in indoor multi-cell VLC systems using optimized angle diversity receiver," J. Lightwave Technol. **36**(17), 3603–3610 (2018).
35. C. Zhu, B. Song, B. Corcoran, L. Zhuang, and A. J. Lowery, "Improved polarization dependent loss tolerance for polarization multiplexed coherent optical systems by polarization pairwise coding," Opt. Express **23**(21), 27434–27447 (2015).
36. J. He, J. He, and J. Shi, "An enhanced adaptive scheme with pairwise coding for OFDM-VLC system," IEEE Photonics Technol. Lett. **30**(13), 1254–1257 (2018).
37. Y. Nie, W. Zhang, Y. Yang, X. Deng, M. Liu, and C. Chen, "Pairwise coded *m*CAP with chaotic dual-mode index modulation for secure bandlimited VLC systems," Photonics **9**(3), 141 (2022).
38. H. G. Olanrewaju, J. Thompson, and W. O. Popoola, "Pairwise coding for MIMO-OFDM visible light communication," IEEE Trans. Wireless Commun. **19**(2), 1210–1220 (2020).
39. C. Chen, Y. Nie, X. Zhong, M. Liu, and B. Zhu, "Characterization of a practical 3-m VLC system using commercially available Tx/Rx modules," in *Proc. Asia Communications and Photonics Conference (ACP)*, (2021), p. W2B.4.